Experimental and Computational Investigation of Aerodynamic Interactions in Quadrotor Configurations

Anna A. Kostek*
Research Scientist

Johannes N. Braukmann
Research Scientist

Felix Lößle
Research Scientist

German Aerospace Center (DLR), Göttingen, Germany

Sebastian Miesner
Research Scientist
University of Stuttgart, IAG
Stuttgart, Germany

Antonio Visingardi
Research Scientist
Italian Aerospace Research Center (CIRA)
Capua, Italy

Ronan Boisard
Research Scientist
French Aerospace Lab (ONERA)
Meudon, France

Vasilis Riziotis
Associate Professor
National Technical University of Athens (NTUA)
Athens, Greece

Manuel Keßler
Group Leader
University of Stuttgart, IAG
Stuttgart, Germany

Anthony D. Gardner
Group Leader
German Aerospace Center (DLR)
Göttingen, Germany

The influence of interactional effects on quadrotor performance in forward flight was evaluated taking into account square and diamond configurations, forward and backward tilt angles, and a range of hub spacings including overlapping blades. The analysis was based on the wind-tunnel measurements and simulations from four midfidelity computational methods and the high-fidelity tool. The outcome indicates that the efficiency of a diamond configuration improves by 5% in comparison with isolated rotors for nonoverlapping rotor spacings, while the interactions in square alignments are detrimental for all analyzed test cases with the optimum at 0.04*D* blade overlap. The trend is more pronounced for the backward rotor tilt with intensified interactions, for which the efficiency of the diamond configuration increases by 11% at 1.2*D* rotor spacing. The computational results showed good agreement with the measurement data for the forward rotor plane tilt; however, for the backward tilt angle, the spread between the calculated values, especially for torque, could be observed with the general trends maintained. The study shows negligible impact of the rotor phasing on the quadrotor efficiency.

Nomenclature

d	distance between rotor hubs of neighboring rotors, m
D	rotor diameter, m
P	required power, W
T, Q	unsteady thrust, N; torque, Nm
$\overline{T}, \overline{Q}$	time-averaged thrust, N; torque, Nm
$T_{\text{single}}, Q_{\text{single}}$	thrust, torque produced by an isolated rotor in corresponding flight conditions
v_z	velocity component perpendicular to the plane, m/s
V	free-stream velocity
ω	angular velocity, rad/s
CFD	computational fluid dynamics
CORAL	Comprehensive Rotorcraft Analyses Lab
DEHS	di-ethyl-hexyl-sebacate
IAG	Institute of Aerodynamics and Gas Dynamics
PIV	particle image velocimetry
PUMA	potential unsteady methods for aerodynamics
RAMSYS	Rotorcraft Aerodynamic Modelling SYStem
RPM	rotations per minute
UAV	unmanned aerial vehicle
UPM	unsteady panel method
URANS	unsteady Reynolds-averaged Navier–Stokes

*Corresponding author; email: anna.kostek@dlr.de.

Presented at the Vertical Flight Society's 79th Annual Forum & Technology Display, West Palm Beach, FL, May 16–18, 2023. Manuscript received April 2023; accepted November 2023.

Introduction

Investigation of interactions between unmanned aerial vehicle (UAV) rotors has become an important research topic as a proper aerodynamic design of a multicopter is a key to maximize its flight performance regarding the low-energy density of current batteries. At the same time, the use of small, fixed-pitch rotors, typical for UAVs, brings into question the applicability of traditional tools developed for full-scale aircraft. The operation at much lower Reynolds numbers not only affects the rotor performance but also has an influence on aerodynamic interactions between the rotors. Shukla and Komerath (Ref. 1) showed experimentally that the close proximity of two rotors in hover causes a decrease in their efficiency at lower rotational speeds. Their following study (Ref. 2) indicates the difference in performance trends for overlapping bi-rotor configurations compared with the high Reynolds number data. Nevertheless, as proved by Hwang et al. (Ref. 3) in the numerical investigation of quadrotors, the interactions between the rotors in hover are limited but become a significant factor in the forward flight. The greatest influence can be observed for cases with wake of the upstream rotor(s) closely passing the rotor plane, which is the case for the higher tilt angles (Ref. 4). Healy et al. (Ref. 5) indicated in the numerical study of a tandem configuration how the disk loading and advance ratio affect the wake skew angle of the front rotor resulting in higher efficiency losses for the downwash rotor at higher flight speeds and lower disk loadings. Changes in the multirotor wake propagation depending on the advance ratio were also presented experimentally with particle image velocimetry (PIV) by Throneberry et al. (Ref. 6).

Another important factor affecting the interrotor interactions is the wake geometry. Fixed-pitch rotors in the forward flights generate

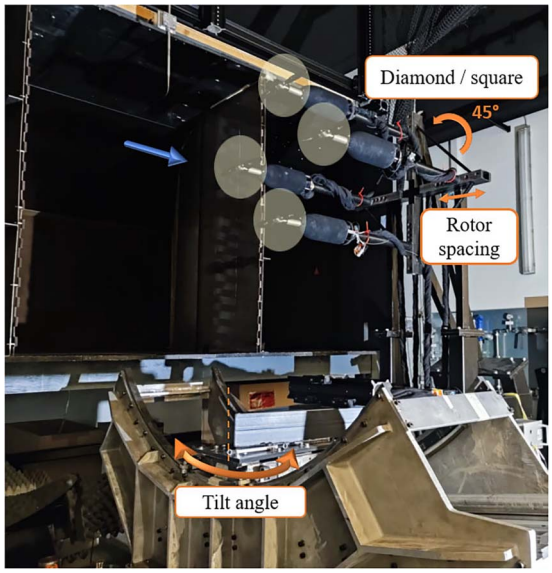

Fig. 1. Experimental setup with investigated parameters.

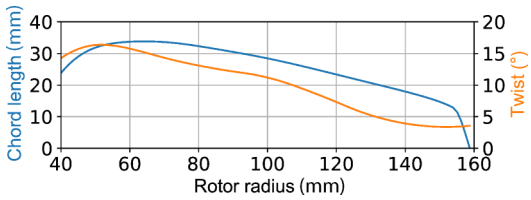

Fig. 2. Twist and chord distributions along the blade radius (Ref. 28).

imbalanced forces between the retreating and advancing sides, which results in the asymmetry of the produced wake. The advancing side tip vortex is stronger but propagates quicker downward than the tip vortex on the retreating side and thus for the regular forward flight conditions stays farther from the rotor plane. Misiorowski et al. (Ref. 7) showed in the numerical study of a diamond (plus) quadrotor configurations that both rolled-up tip vortices of the front rotor have a positive effect on the performance of the side rotors. As a result, the diamond alignment shows a better efficiency than a square (cross) configuration, which was proved in the calculations of Hwang et al. (Ref. 3), also using a potential method in the study of Barcelos et al. (Ref. 4). However, the plus configuration requires larger control inputs to compensate for additional moments and indicates 30% lower control authority as estimated by Niemiec and Gandhi (Ref. 8).

A negative impact of the downwash on the back rotors in the square configuration can be reduced by increasing the horizontal rotor spacing, as shown in the wind tunnel measurements and flight tests by Atte et al. (Ref. 9). However, Healy et al. (Ref. 5) presented for the tandem configuration that increasing the vertical offset is a more effective solution. The numerical study of the SUI Endurance quadcopter by Ventura Diaz and Yoon (Ref. 10) indicated a 63% thrust increase achieved by undermounting the front rotors. An alternative approach was suggested in the following investigation by Healy et al. (Ref. 11), which shows that outward longitudinal canting of the rotors can reduce the lift deficit on the back rotor together with the pitching moment.

Introducing the vertical offset allows for the design of the overlapping rotors and thus more compact configurations, which, however, brings an increase in the aerodynamic interactions. A few studies have been done for such cases, mostly focused on the hover (Refs. 2, 12) or axial flight performance (Ref. 13). Nevertheless, the overlapping rotors are also applicable in the edgewise flow conditions, as in the case of the novel design of the overlapped quadrotor tested by Chen et al. (Ref. 14).

Regarding an increasing interest in the use of multirotor systems, either small-scale UAVs or man-sized urban air mobility aircraft, in densely populated areas, the ability to evaluate and understand their noise characteristics has become another important topic of research (Refs. 15, 16). Zhou et al. (Ref. 17) investigated twin-rotor hover cases, for which the proximity of the rotors resulted in small changes in the thrust coefficient (within 2%); however, a significant increase in the thrust fluctuations could be observed with reduced hub spacing. This in turn, together with turbulent flow interactions, increased the aeroacoustic noise levels up to 3 dB. The change in aeroacoustic characteristics of the multirotor with closer rotor positioning was also investigated by Lee and Lee (Ref. 18) and Ko et al. (Ref. 19). Intaratep et al. (Ref. 20) and Tinney and Sirohi (Ref. 21) studied the interactions leading to an increase in noise levels due to increasing number of rotors. Zhou and Fattah (Ref. 22) presented the influence of canting in a two-rotor system on the sound directivity and, as later confirmed by Smith et al. (Ref. 23), emphasized the importance of rotor phasing for noise reduction.

Along with the aerodynamic performance, the acoustic emission of rotors varies depending on different design parameters and flight conditions and requires separate investigations by means of robust and reliable computational methods. Even though the complexity of the multirotor flow can be captured with computational fluid dynamics (CFD) codes (Ref. 24), consideration of interactional effects in the initial steps of the aircraft design process is feasible only by using lower fidelity tools. Niemiec and Gandhi (Ref. 25) developed a blade element theory method to analyze quadrotor dynamic behavior in hover and forward flight. Even though the presented low-fidelity approach considerably reduces the computational costs, it is not capable of capturing the interactional effects between the rotors. Pinti et al. (Ref. 26) suggested a solution to analyze the influence of different longitudinal and vertical spacings in the tandem configuration, in which the low-fidelity tool was used for identifying the key parameters to perform more accurate high-fidelity calculations in the next step. Conley and Shirazi (Ref. 27) validated the results of multirotor performance from two midfidelity tools with experimental data. As shown, such methods can offer a compromise between computational cost and accuracy. Nevertheless, it is important to study the reliability and possible error margins of lower cost simulations for the broad spectrum of design parameters.

The presented study offers a basis for comparison between four midfidelity methods and a high-fidelity tool for simulations of different quadrotor configurations in the forward flight, validated with experimental data. The test matrix includes a wide range of rotor distances and varying tilt angles of the rotor plane, including the high interaction cases with overlapping blades without a vertical rotor offset and backward tilt angles. The analysis covers changes in thrust and torque relative to the loads of an isolated rotor for each tool as well as the comparison of induced velocity fields with PIV measurements for the selected cases. The investigation of two-rotor systems serves a better understanding of the interactional effects and possible solver limitations.

The project is an extension of a single UAV rotor study (Refs. 28, 29).

Experimental Setup and Rotor Geometry

The quadrotor experiment was conducted in the Rotor Test Facility Göttingen at the German Aerospace Center (DLR) with the setup presented in Fig. 1. Fixed-pitch, two-bladed KDE 12.5 × 4.3 inch rotors (Fig. 2) were used in the investigation operating with a constant rotational speed of 5400 RPM at a wind velocity of 12.9 m/s. The analyzed

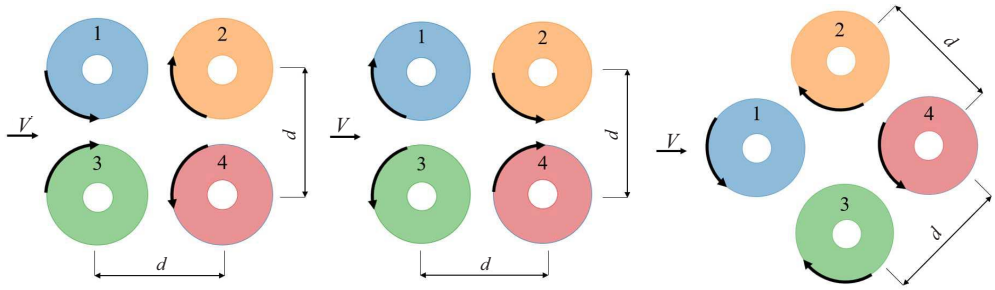

(a) Square bearhug (b) Square breaststroke (c) Diamond

Fig. 3. Analyzed quadrotor configurations.

(a) Tilt −10° (b) Tilt 10°

Fig. 4. Tilt angle sign convention.

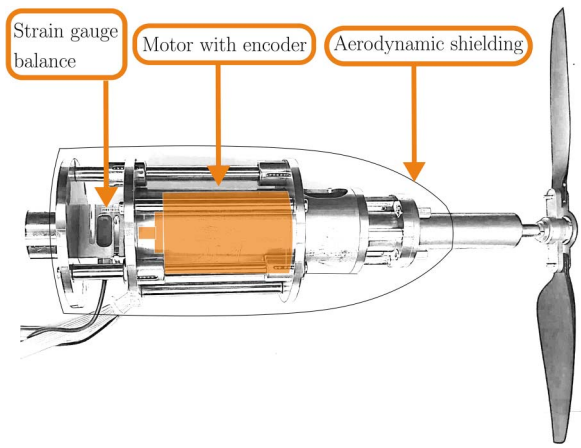

Fig. 5. Setup of the drive unit.

conditions correspond to the rotor advance ratio of 0.146 with a tip Mach number of 0.259 and the Reynolds number on the order of 10^4 to 10^5 across the rotor disk.

Strain gauge balances were used to measure the individual thrust of each rotor and torque values were derived from electric energy consumption based on the motor efficiency data. A rotatable frame allowed for the analysis of both square and diamond configurations with an alteration of rotation direction for the latter (Fig. 3). The measurements of each configuration involved variations of horizontal rotor spacing in seven steps with the largest distance of 1.68D between the rotor hubs and the closest positioning with 0.26D rotor overlap. For each spacing, the tilt angle of the rotor plane was scanned between −30° and 30° with negative angles, representing a forward tilt of the rotor plane and positive angles meaning a backward tilt, as shown in Fig. 4. In order to better understand the interactional effects depending on the rotor alignment, the number of operating rotors was alternated between 1, 2, and 4 for selected hub distances.

The drive unit of each rotor consisted of a Maxon EC-i52 motor with an encoder 16 EASY, mounted as shown in Fig. 5. The master-slave motor operation mode implemented using EPOS2 70/10 controllers enabled a constant orthogonal rotor phasing as well as the same acceleration of the rotors necessary for the operation in overlapping positions. Downwash velocities were measured using PIV for a tilt angle of −10° and a reduced set of test points. For this purpose, a light sheet parallel to the rotor plane, 75 mm downstream was generated by two lasers with a wavelength of 532 nm and a combined pulse energy of 200 mJ. The test section was seeded using a di-ethyl-hexyl-sebacate (DEHS) aerosol with an approximate droplet diameter of 2 μm. Two PCO.edge cameras with a resolution of 2560×2160 pixels, equipped with lenses with a focal length of 35 mm were used for image recording (Fig. 6). The cross-correlation of the images was performed using an iterative approach by reducing interrogation window size from 48 × 48 pixels in the initial pass to 16 × 16 pixels in the final pass. Given the applied window overlap of 75%, this results in a spatial resolution of 3.35 vectors/mm in the vector fields. The images were recorded with a recording frequency slightly below 3.75 Hz leading to a small phase offset of the rotor in each PIV image. The frequency offset was adjusted to result in approximately 1000 images evenly distributed over the rotor azimuth. Areas lacking illumination due to the shadows of the rotor axes and areas covered by the rotors were masked out before averaging the captured data for each test case and appearing as white regions in the presented velocity maps.

Computational Methods

The study presents a comparison of results calculated with four mid-fidelity tools and a high-fidelity method.

The unsteady panel method (UPM) (DLR) is an unsteady free-wake panel method solving potential flow (Ref. 30). In the presented study the wake was represented by the vortex lattice, and no postprocessing viscous corrections were applied to the results. The applied blade model consisted of 15 spanwise and 95 chordwise panels (Fig. 7(a)). Calculations were performed with a time step corresponding to a 2° azimuthal increment.

Rotorcraft Aerodynamic Modelling SYStem (RAMSYS) Italian Aerospace Research Center (CIRA) represents another midfidelity code for multirotor and multibody configurations (Ref. 31). It is based on the boundary element method for solving unsteady, inviscid, and incompressible flows. The velocity potential on the blades is calculated using Morino's boundary integral formulation to Laplace's equation (Ref. 32) and then used to evaluate pressure distribution by means of the unsteady Bernoulli equation. Calculations were made with an azimuth step of 2° and considering six rotor revolutions and six wake spirals.

Potential unsteady methods for aerodynamics (PUMA) (ONERA) is an unsteady lifting-line, free-wake solver. In this method, the wake is modeled by a potential discontinuity surface according to Mudry theory (Ref. 33) and includes corrections for blade sweep and dynamic stall models. In the presented study, the viscous and compressible effects were accounted for based on two-dimensional airfoil characteristics. In

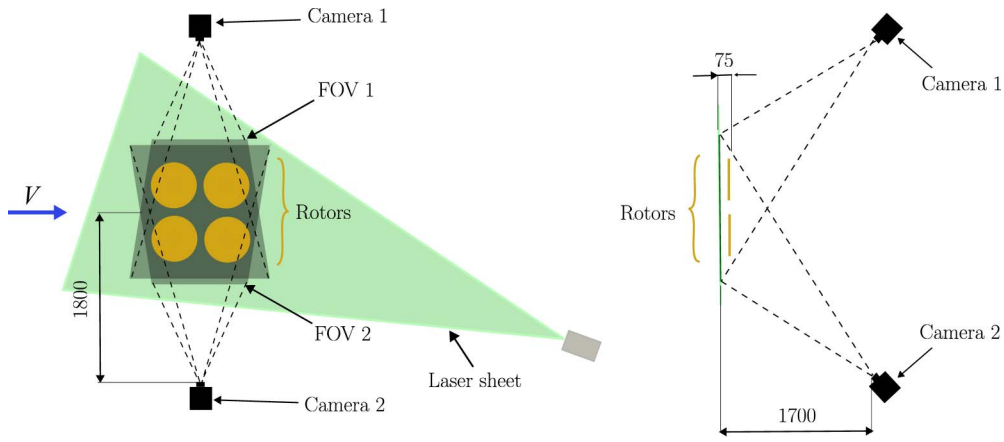

Fig. 6. PIV setup presented for the square configuration with a top view (left) and side view (right) relative to the rotor plane.

(a) UPM - 'thick' blade **(b) CORAL - lifting surface**

Fig. 7. Applied blade models.

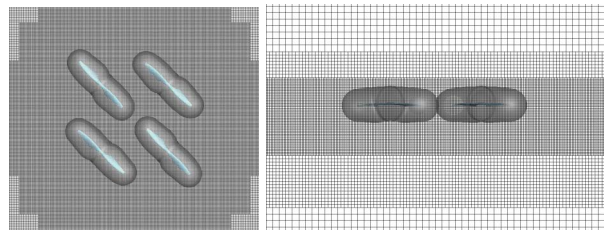

(a) Top view **(b) Side view**

Fig. 8. Computational mesh in FLOWer.

Ref. 28, the method was shown to be very robust compared to UPM but the quality of the results depends strongly on the quality of the airfoil polars delivered by DLR. The lifting line consisted of 45 radial stations with square root distribution. Calculations were conducted with a 5° azimuthal step.

The Comprehensive Rotorcraft Analyses Lab (CORAL) National Technical University of Athens (NTUA) is a joint effort of Roma Tre – RM3 University, NTUA, Carleton University's Rotorcraft Research Group – CU under the coordination of Kopter Germany, a member of Leonardo group. It includes tools for the combined aeroelastic and aeroacoustic analyses of helicopter configurations (Ref. 34). The aerodynamic part of the code consists of models of varying fidelity including free wake vortex particle modules and an Unsteady Reynolds-averaged Navier–Stokes (URANS) hybrid CFD module. The free vortex wake models solve the inviscid-incompressible-unsteady flow equations around lifting/or nonlifting bodies which can be treated either as lifting-lines, lifting surfaces, or thick panel bodies (lifting and nonlifting). The presented results were prepared with the lifting surface modeling option with no correction from airfoil polars and a step size of 4°. The hybrid wake consisted of a vortex lattice for the first 1/6 of the revolution and was then converted into vortex particles. The blade model consisted of 20 spanwise and 15 chordwise elements (Fig. 7(b)).

High-fidelity calculations were performed with a structured CFD code FLOWer (IAG) (Ref. 35). The method used sixth-order spatial weighted essentially non-oscillatory scheme and the Wilcox k-ω turbulence model (Ref. 36). The time step corresponded to 0.5° rotor azimuth. The applied setup consisted of 32.4 million cells with 2.4 million in eight blade meshes and 8.7 million in the background. The rotor blades were embedded via the Chimera technique into the Cartesian off-body mesh with a refined area downwash below the blades to capture the rotor wake (Fig. 8). The boundary layer of the rotor blades was fully resolved by ensuring $y^+ < 1$ on the whole surface.

The main settings used in the computations with different methods are collected in Table 1.

Reference Results of an Isolated Rotor

Selected results of a single rotor performance from the measurement and calculations (Table 2) served as a reference for the analysis of interactional effects in multirotor configurations operating in corresponding flight conditions and were described in detail in the preceding investigation (Ref. 28). The quadrotor analysis was focused on two tilt angles representing a regular orientation of an aircraft in the forward flight ($-10°$) and a braking mode ($+10°$). For the latter strong interactional effects arise from rotors being affected by their own wake as well as enhanced blade–wake interactions between the rotors.

The performed calculations indicate that the analyzed fixed-pitch rotor in the forward flight sheds an asymmetric wake due to imbalance of forces across the rotor disk (Fig. 9). With a rotor tilted forward, a strong, wide vortex from the advancing side propagates quickly downward, while a weaker tip vortex from the retreating side stays longer in the vicinity of the blades. The induced velocity field captured by the PIV in Fig. 10 shows a strong advancing side downwash inboard (in blue), together with asymmetric upwash regions (in orange) on the outboard blade areas coming from the rolled-up tip vortices from both sides. This behavior has an influence on the interaction between the rotors depending on their mutual position.

Two-Rotor System Analysis

The analysis of two-rotor configurations served for a better understanding of the nature of the interactional effects as well as an initial assessment of capabilities of chosen solvers to recreate these effects. Therefore, the influence of tilt angle change and rotor spacing on the rotor performance was primarily investigated. The selected alignments of two rotors represent parts of quadrotor systems in square and diamond configurations (Figs. 11–13).

Table 1. Summary of main computational settings

	Blade Model	Wake Model	Flow Assumptions	Time Step
UPM	15×98 elements thick blade	Free-wake, vortex lattice	Potential	2°
RAMSYS	15×50 elements thick blade	Free-wake, vortex lattice	Potential	2°
PUMA	45 elements lifting line	Free-wake, vortex lattice	Potential, airfoil polars: viscous and compressible	5°
CORAL	15×20 elements lifting surface	Free-wake, hybrid	Potential	4°
FLOWer	2.4 million elements thick blade	URANS	Viscous, compressible, rotational	0.5°

Table 2. Thrust of a single rotor, 5400 RPM, V = 12.9 m/s, and tilt angle −10°

		Experiment (Ref. 28)	UPM	FLOWer	RAMSYS	PUMA	CORAL
Thrust (N)	−10°	7.37	7.13	6.43	7.048	7.13	6.41
	+10°	10.19	10.08	9.38	9.73	9.91	9.09
Torque (Nm)*	−10°	0.09	0.081*	0.095	0.083*	0.099	0.074*
	+10°	0.064	0.057*	0.075	0.061*	0.082	0.055*

*Inviscid.

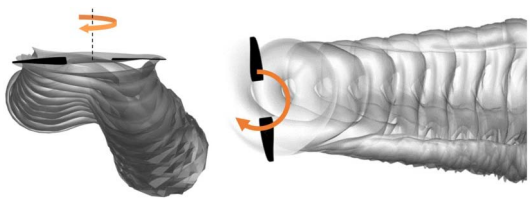

(a) Front view (b) Top view

Fig. 9. Wake of an isolated rotor at a tilt angle −10° visualized in UPM.

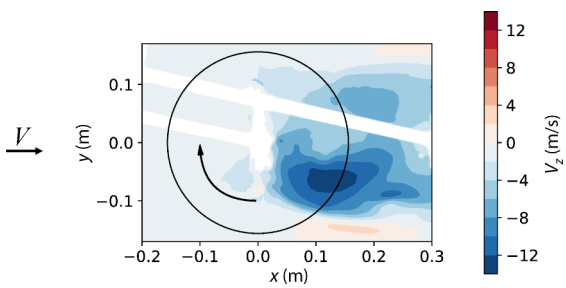

Fig. 10. Downwash of a single rotor captured with PIV for tilt −10°; white areas come from rotors and hubs' shadows, where data were not evaluated.

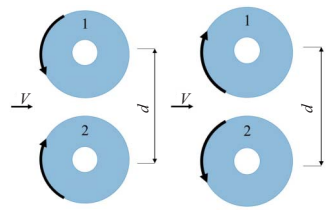

(a) Bearhug (b) Breaststroke

Fig. 11. Rotors side-by-side.

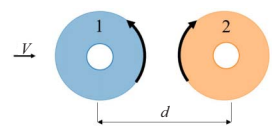

Fig. 12. Tandem.

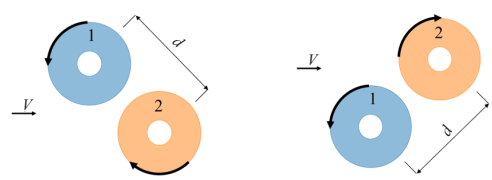

(a) Diagonal bearhug (b) Diagonal breaststroke

Fig. 13. Rotors in oblique alignment.

Side-by-side alignment

Two counterrotating rotors were aligned side by side with either their advancing or retreating sides meeting, forming, respectively, the bearhug or breaststroke configuration (Fig. 11). By definition this system is symmetric relative to the flow, so the same effects affect each rotor. Hence, the presented results apply to both rotors 1 and 2. The side-by-side positioning has a beneficial influence on rotor performance (Fig. 14) with up to 10% gain in thrust and roughly 20% torque reduction compared to an isolated rotor case for $d/D = 0.96$ (Fig. 14). The velocity distribution shown in Fig. 15 with respect to an isolated rotor indicates upward flow regions between the rotors (in red) caused by an interaction of their rolled-up tip vortices. The created upwash leads to a simultaneous increase in thrust and a decrease in induced drag at around 90° azimuth for both rotors (Figs. 16 and 17). Differences between the results of bearhug and breaststroke are apparent for high-interaction cases like closer rotor positions and positive tilt angles, for which a breaststroke configuration, with stronger advancing side vortices interacting (Fig. 15(b)), is more favorable. Considerable, beneficial effects can be noticed for very close rotor spacings around $d/D = 1$ (compare Figs. 16(a) and 16(b)); however, a deeper overlap of the blades causes detrimental interactions with the inboard downwash of the neighboring rotor.

The potential solver UPM showed good agreement with experimental results and FLOWer as for the thrust increase evaluation, while it tends to strongly overestimate the interactional effects on the torque for high positive tilt angles (Fig. 14(b)).

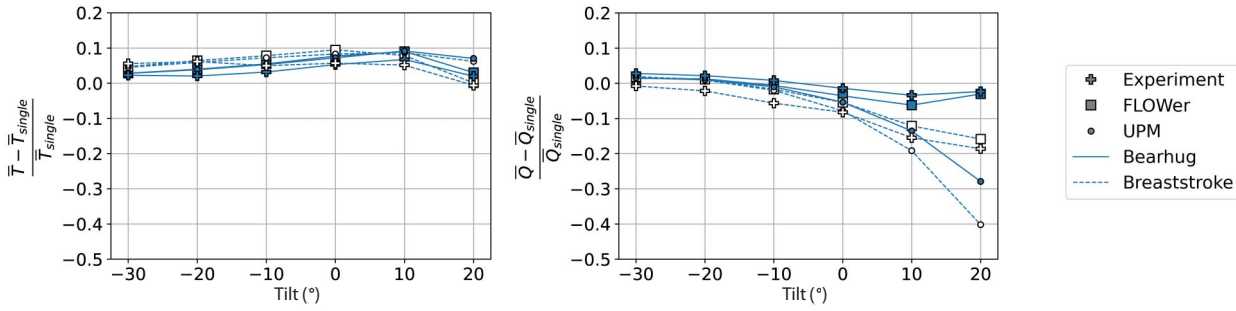

(a) Relative thrust change (b) Relative torque change

Fig. 14. Effects of varying tilt angle on rotor performance in side-by-side alignment for $d/D = 0.96$.

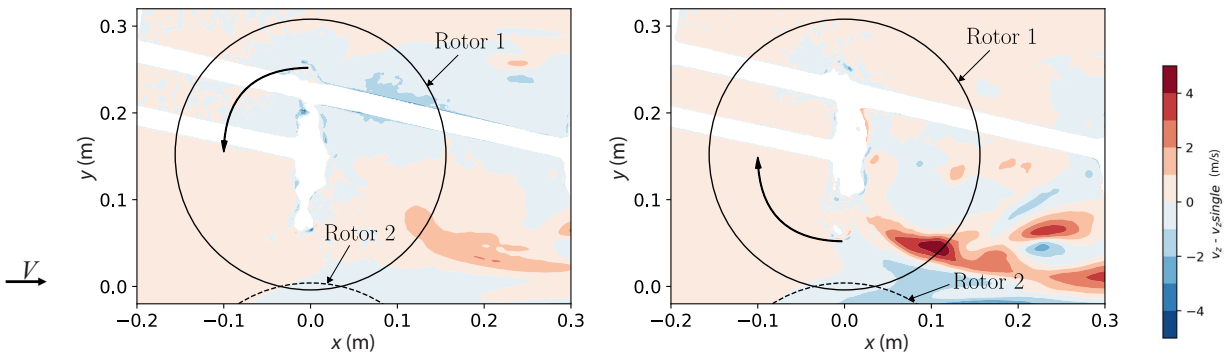

(a) Bearhug (b) Breaststroke

Fig. 15. Upwash regions between the rotors in side-by-side interaction, captured with PIV relative to an isolated rotor measurement for $d/D = 0.96$ and tilt −10°; white areas come from rotors and hubs' shadows, where data were not evaluated.

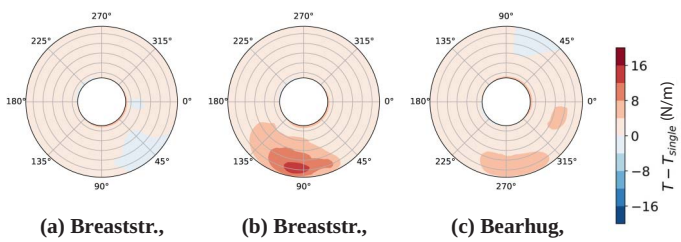

(a) Breaststr., $d/D = 1.2$ (b) Breaststr., $d/D = 0.96$ (c) Bearhug, $d/D = 0.96$

Fig. 16. Effect of side-by-side alignment with tilt −10° on thrust of rotor 1 (UPM).

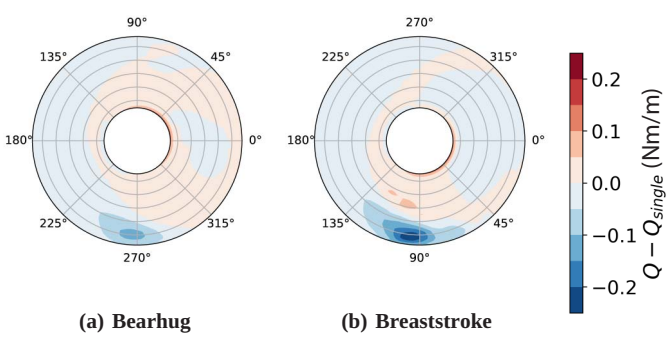

(a) Bearhug (b) Breaststroke

Fig. 17. Effect of side-by-side alignment with tilt −10° on the torque of rotor 1, $d/D = 0.96$ (UPM).

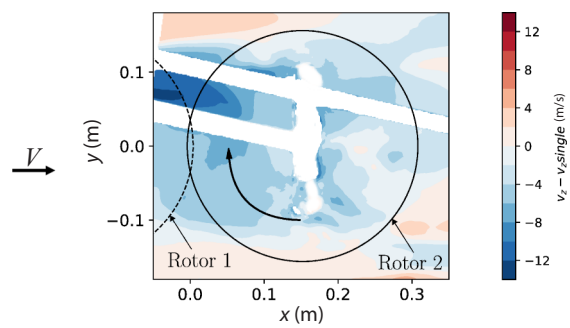

Fig. 18. Change in downwash of rotor 2 in tandem interaction relative to an isolated rotor, captured with PIV for $d/D = 0.96$ and tilt −10°; white areas come from rotors and hubs' shadows, where data were not evaluated.

Tandem

In a tandem configuration, rotor 2 is positioned directly behind rotor 1 relative to the flight direction (Fig. 12). As shown on the PIV plane in Fig. 18, the front of rotor 2 is affected by the downwash of rotor 1 (blue color), while around 90° and 270° azimuth it may operate locally in the upwash from the tip vortices of rotor 1 (orange color). The proximity to rotor 2 has a beneficial, yet negligible, impact on the front rotor's performance as shown for $d/D = 1.2$ (Fig. 19). On the other hand, even for cases with a forward tilt of the rotor plane, rotor 2 is heavily affected by the downwash of the preceding rotor causing a considerable decline in its efficiency with minimum 10% loss. The interactional effects intensify

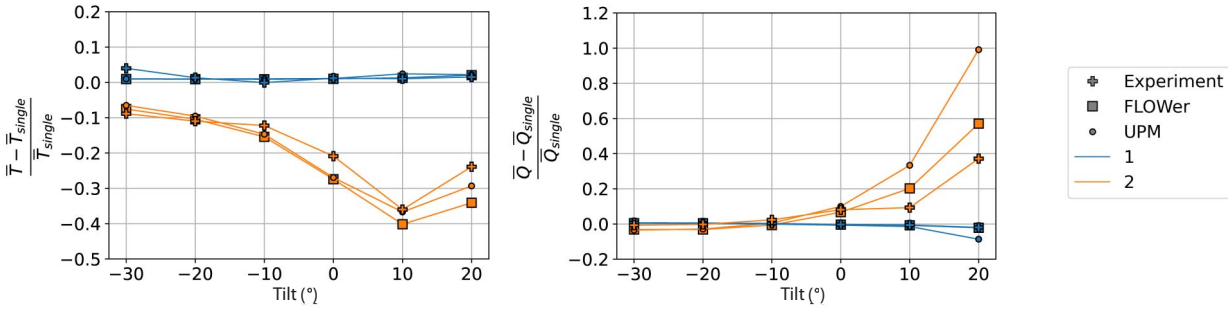

(a) Relative thrust change **(b) Relative torque change**

Fig. 19. Effects of varying tilt angle on rotor performance in tandem for $d/D = 1.2$.

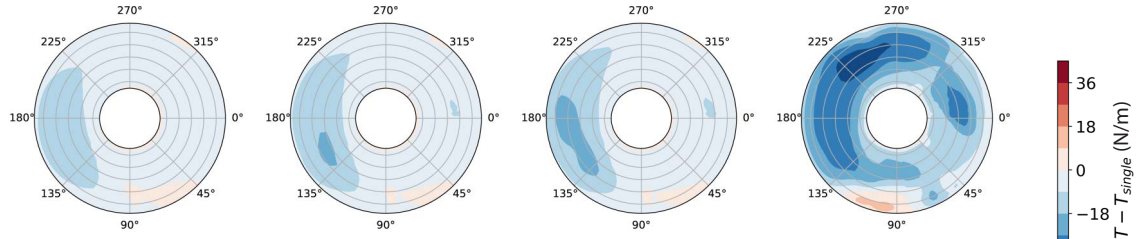

(a) Tilt −10°, d/D = 1.2 **(b) Tilt −10°, d/D = 1.04** **(c) Tilt −10°, d/D = 0.96** **(d) Tilt +10°, d/D = 1.2**

Fig. 20. Effect of tandem alignment on thrust of rotor 2 (UPM).

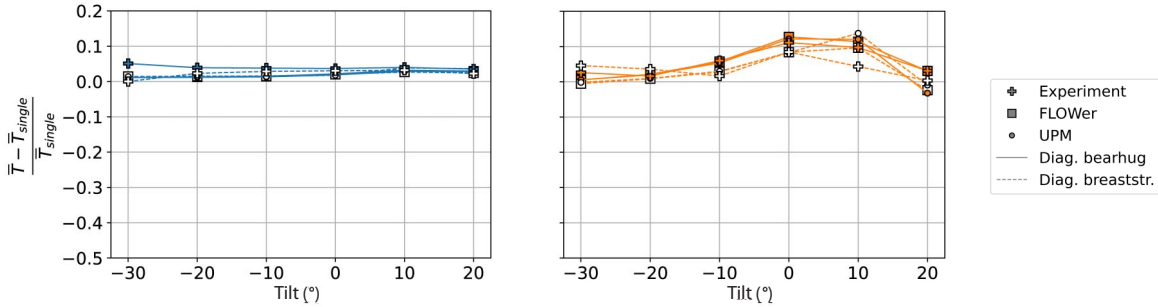

(a) Rotor 1 **(b) Rotor 2**

Fig. 21. Relative thrust change with varying tilt angle in oblique alignment for $d/D = 1.2$.

with decreasing distance between the rotors; however, the increase in a tilt angle has a stronger influence leading to the thrust reduction of roughly 40% for rotor 2 at 10° tilt (Figs. 19(a) and 20). In this case, rotor 2 is located directly in the wake of the preceding rotor experiencing strong downwash, especially from the advancing side of rotor 1. As the advancing side tip vortex of rotor 1 reaches the plane of the rear rotor, an upwash region can be observed around azimuth 90° of rotor 2, yet it does not significantly improve its performance (Fig. 20(d)).

FLOWer and UPM results show similar tendencies as the experiment when it comes to the thrust changes; however, both tools overestimate the relative torque increase for rotor 2 at higher tilt angles (Fig. 19(b)).

Oblique alignment

In the oblique alignment, rotor 2 is located behind rotor 1, on its retreating side for "diagonal bearhug" or advancing side for "diagonal breaststroke" (Fig. 13). The interaction with the tip vortices of the preceding rotor has a positive impact on rotor 2 for both configurations, especially for higher tilt angles as the vortices raise closer to the level of the rear rotor (Figs. 21 and 22). The effect is greater and observable already for moderate tilt angles for the diagonal bearhug alignment as the retreating side tip vortex of rotor 1 propagates closer to the rotor plane. The advancing side tip vortex in the diagonal breaststroke configuration creates the strongest upwash on rotor 2 at around 10° tilt angle, possibly leading locally to the stall conditions on its blades, which cannot be captured by the potential solver UPM (Fig. 21(b)). Consequently, UPM tends to overestimate the interactional effects on torque of rotor 2 for higher tilt angles (Fig. 22(b)). The impact of the interaction on the front rotor is much less prominent; however, a slight improvement in its efficiency can be observed with a simultaneous gain in thrust and torque reduction of up to 5% for 20° tilt.

The positive impact on the rear rotor in oblique alignment decreases for higher tilt angles and closest rotor positions as rotor 2 starts to partially operate in the downwash from the inner wake of rotor 1 (blue in Fig. 23). This results in the regions of locally reduced thrust and

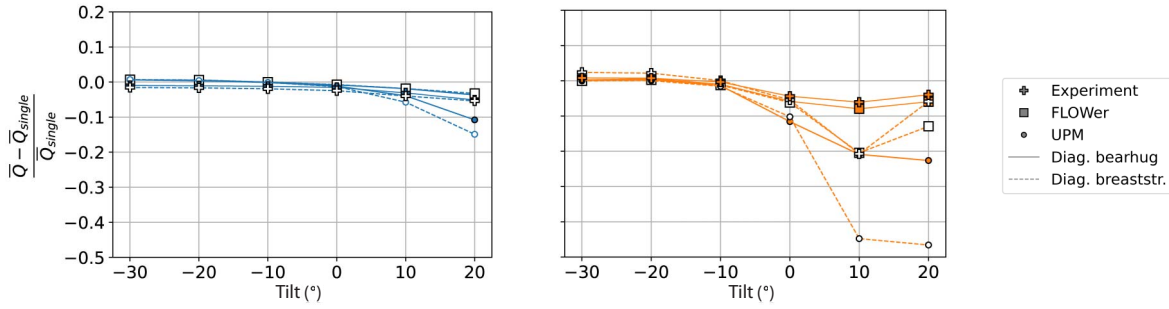

(a) Rotor 1 (b) Rotor 2

Fig. 22. Relative torque change with varying tilt angle in oblique alignment for $d/D = 1.2$.

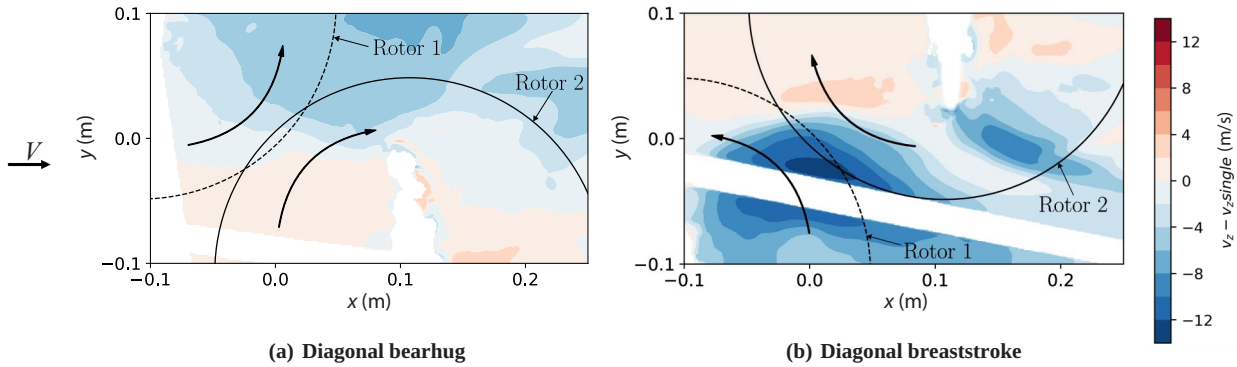

(a) Diagonal bearhug (b) Diagonal breaststroke

Fig. 23. Downwash of rotor 2 in oblique interaction relative to an isolated rotor, captured with PIV for d/D = 0.96 and tilt −10°; white areas come from rotors and hubs' shadows, where data were not evaluated.

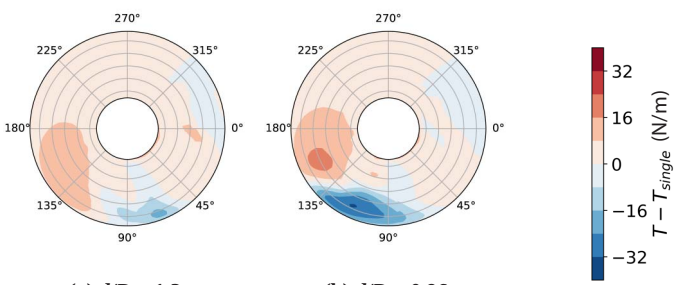

(a) d/D = 1.2 (b) d/D = 0.96

Fig. 24. Effect of diagonal breaststroke alignment with tilt 0° on thrust of rotor 2 (UPM).

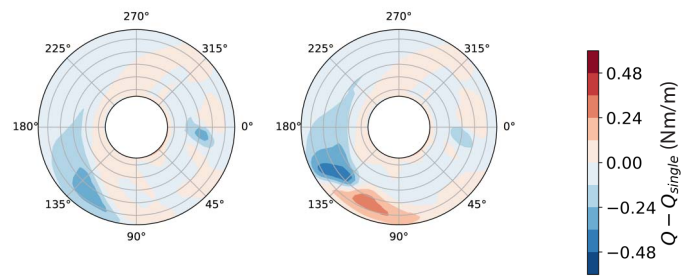

(a) d/D = 1.2 (b) d/D = 0.96

Fig. 25. Effect of diagonal breaststroke alignment with tilt 0° on torque of rotor 2 (UPM).

simultaneously increased torque as shown for 0° tilt in Figs. 24 and 25 for the diagonal breaststroke configuration.

Quadrotor Analysis

The analysis of interactional effects for each configuration was done based on a comparison of total thrust and torque generated by the quadrotor system with that obtained by four isolated rotors (Figs. 26 and 27). All applied computational methods and measurements illustrate the same trends due to the change in the hub spacing for a forward tilt angle of −10° with a maximum difference of 4% between the exact values. Results indicate that interactions appearing in the square alignment are detrimental for all of the analyzed rotor spacings; however, a small overlap of blades is around 3% more beneficial than wider hub separations. The most overlapping rotor positioning leads again to a decrease in thrust up to 10%, yet a reduction of torque by around 5% also occurs in this region. For larger hub spacings and forward tilt of the rotor plane, the interactional effects on torque are negligible.

While a loss of around 4% of thrust can be observed already for spacing 1.68D for both bearhug and breaststroke configurations, the bearhug system becomes slightly more efficient as rotor spacing decreases. For a positive tilt angle of 10°, the performance of both square systems significantly declines for wider rotor spacings due to thrust reduction by 15% and simultaneous increase of torque by around 10%. Interestingly, the performance of bearhug and breaststroke configurations continuously improves with decreasing rotor spacing with the optimum reached for 0.84D. Moreover, in these conditions, the breaststroke configuration shows better efficiency than the bearhug system.

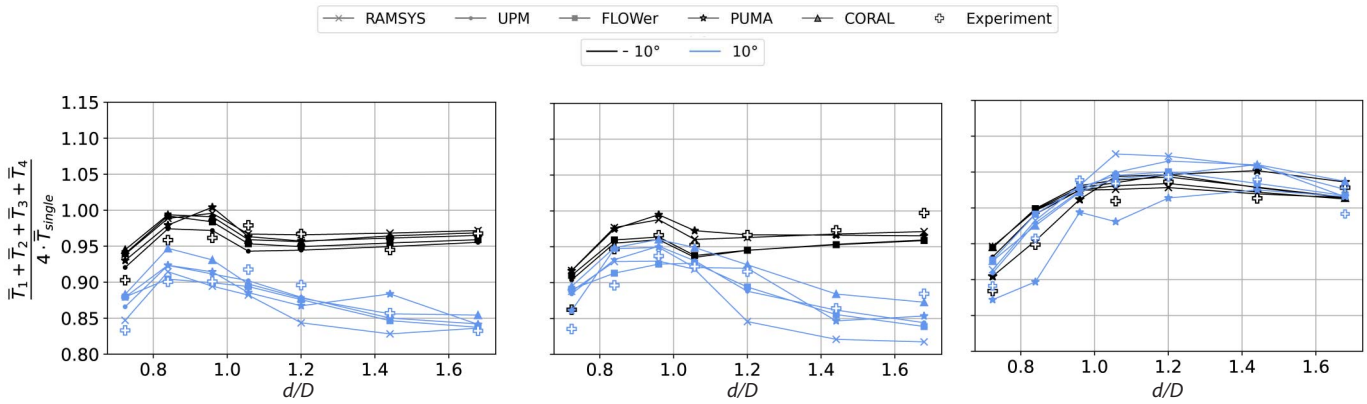

(a) Square bearhug (b) Square breaststroke (c) Diamond

Fig. 26. Change in mean thrust of a quadrotor system with varying rotor spacing.

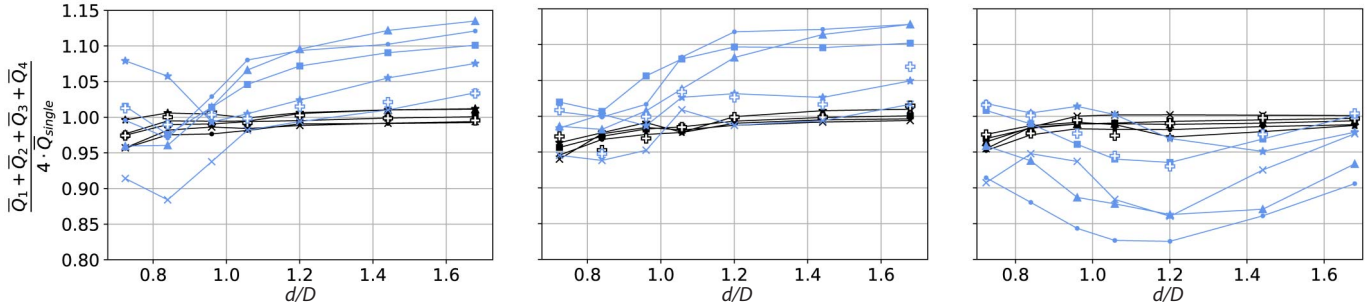

(a) Square bearhug (b) Square breaststroke (c) Diamond

Fig. 27. Change in mean torque of a quadrotor system with varying rotor spacing.

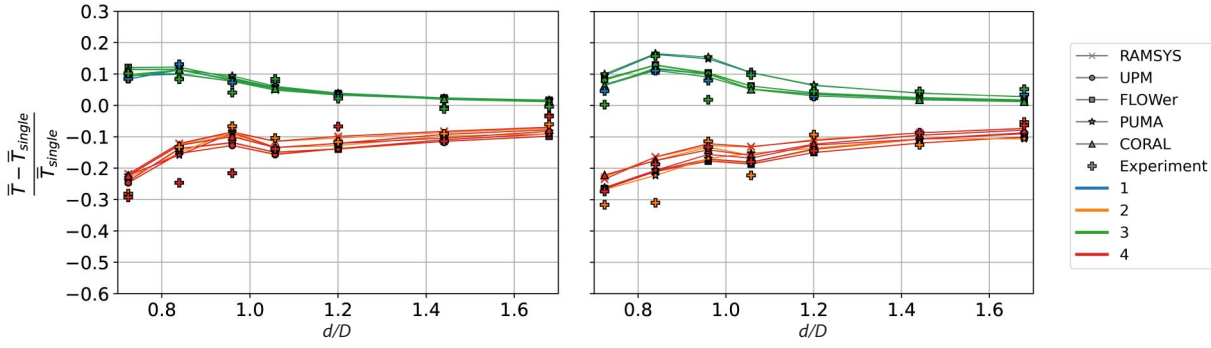

(a) Square bearhug (b) Square breaststroke

Fig. 28. Change in mean thrust of each rotor with varying rotor spacing for tilt angle −10°.

In contrast to square configurations, the results for the diamond system indicate beneficial interactional effects for most of the rotor spacings. The optimal point is reached around 1.2D, where the quadrotor produces 5% more thrust than the isolated rotors. With a further decrease in hub spacing, the performance of a diamond system deteriorates and for positions with the greatest overlap its efficiency is comparable with the square configurations. At tilt +10°, the effect on rotor thrust remains similar to the forward tilt case; however, a reduction in torque can be observed with the minimum occurring for distance 1.2D.

Although all computational tools agree again when it comes to capturing trends at a positive tilt angle, much greater discrepancy is observable in terms of the exact values. The results differ by a maximum of 8% in the assessment of thrust change and up to 15% in the torque estimation.

Square configurations

The effects described for the quadrotor system can be explained by the analysis of the performance change of each rotor individually (Figs. 28–30). As the square alignment is aerodynamically longitudinally symmetric, both front and back rotors show the same changes in efficiency due to interactional effects. The system performance is mostly affected by the downwash from the front rotors, which reduces the thrust produced by rotors 2 and 4 by up to 20% for tilt angle −10° (Fig. 28).

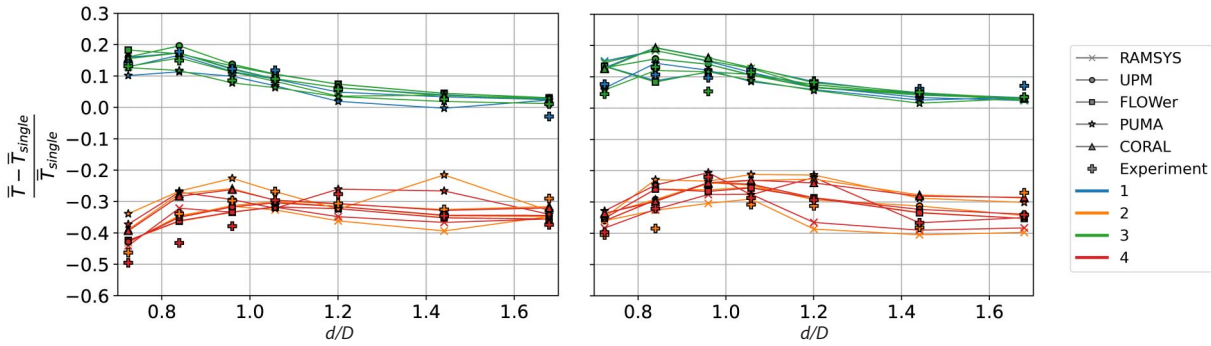

(a) Square bearhug **(b) Square breaststroke**

Fig. 29. Change in mean thrust of each rotor with varying rotor spacing for tilt angle +10°.

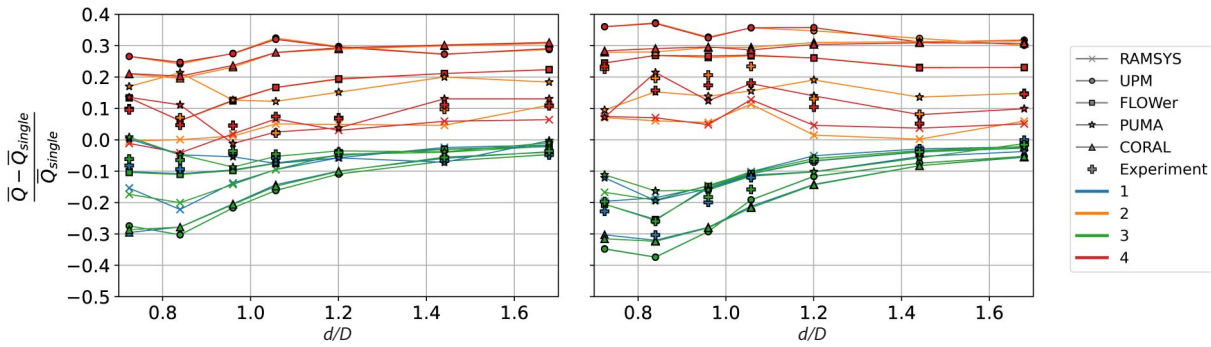

(a) Square bearhug **(b) Square breaststroke**

Fig. 30. Change in mean torque of each rotor with varying rotor spacing for tilt angle +10°.

Similarly to a tandem configuration, the decrease in rotor spacing worsens the performance; however, the increase in the rotor tilt angle has a major influence. For a positive tilt angle of +10°, the thrust produced by the rear rotors drops by up to 40% (Fig. 29). Interestingly, at a negative angle for the smaller hub separations, the efficiency of the rear rotors in the square bearhug configuration is slightly improved compared with the square breaststroke system. For a positive tilt angle, a reverse effect can be observed.

The described trend results partially from a change in the wake geometry of the front rotors due to their mutual interaction. As the separation between rotor 1 and 3 decreases, their tip vortices connect into a supervortex forming a strong upwash region. The connected vortex propagates upwards with this tendency being more apparent in the bearhug configuration for two retreating side tip vortices interacting (Fig. 31). As a result, the downwash effects deteriorating the performance of the rear rotors are slightly reduced in the square bearhug system compared with the square breaststroke for tilt angle −10° (Fig. 32(b)). For rotor spacing, 0.96D rear rotors reach maximum efficiency due to the side-by-side breaststroke interaction appearing around 90° azimuth. A slight improvement in the performance of rear rotors at this rotor separation also appears for the square breaststroke configuration; however, the side-by-side bearhug interaction between rotor 2 and 4 is weaker, as shown in the two-rotor analysis (Fig. 32(d)). With the rotor separation further decreasing, the performance of rotors 2 and 4 strongly deteriorates as it is more affected by the downwash from the inner wake of the proceeding rotor and the rotor on the side (Fig. 32(c)).

For tilt angle +10°, the difference in the rear rotors' efficiency between both square configurations results mostly from the interaction with outer tip vortices of the preceding rotors. In the case of the square

(a) Front view **(b) Side view**

Fig. 31. Comparison of the front rotor wake propagation in square bearhug (blue) and square breaststroke (green).

breaststroke configuration, the retreating side vortices from rotors 1 and 3 reach the level of rotors 2 and 4 creating an upwash region around 90° azimuth and locally improving rear rotors' performance (Fig. 33(b)). On the other hand, the wider and stronger advancing side vortex causes an intensified downwash on the rear rotors in the square bearhug configuration around 225° azimuth (Fig. 33(a)).

For both square configurations, results indicate similar tendencies for the front rotors and show the improvement in their efficiency arising from interactional effects. The thrust produced by rotors 1 and 3 increases with reducing hub spacing by up to 10% for −10° tilt angle and even 20% for +10° tilt. The beneficial effects originate from both tandem and side-by-side interactions, especially visible for close rotor positioning (Fig. 34).

The discrepancies between the selected solvers were analyzed in greater detail for the square breaststroke configuration at rotor spacing 1.2D and −10° tilt angle based on the induced velocity fields (Fig. 35). The blue and red colors represent downwash and upwash regions, respectively, and the white areas in the measurement results come from the shadows of the rotor hubs, for which no velocity data could be evaluated. All of the presented results indicate similar wake propagation;

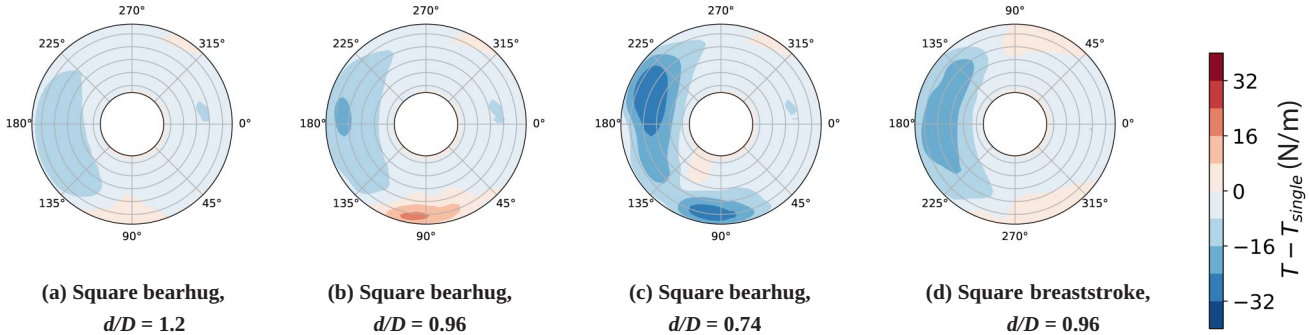

(a) Square bearhug, d/D = 1.2 **(b) Square bearhug, d/D = 0.96** **(c) Square bearhug, d/D = 0.74** **(d) Square breaststroke, d/D = 0.96**

Fig. 32. Change in thrust of rotor 2 in the square configuration with −10° tilt (UPM).

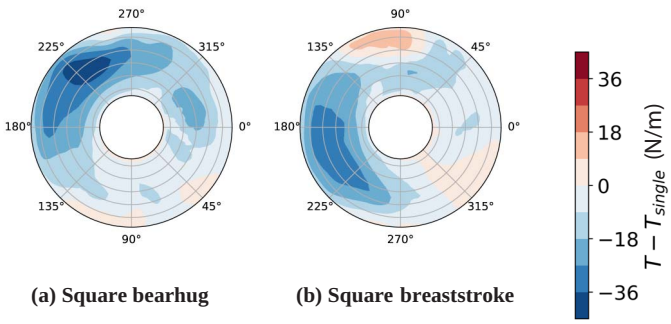

(a) Square bearhug **(b) Square breaststroke**

Fig. 33. Change in thrust of rotor 2 in the square configuration with tilt +10° and $d/D = 0.96$ (UPM).

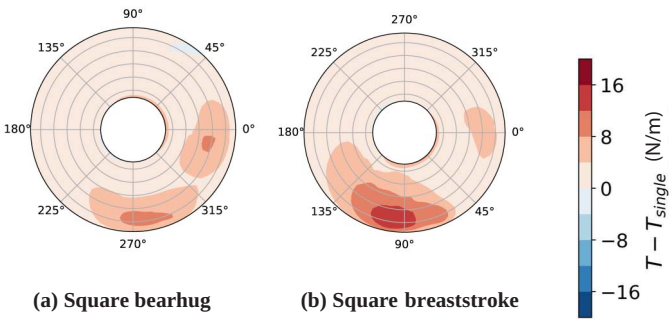

(a) Square bearhug **(b) Square breaststroke**

Fig. 34. Change in thrust of rotor 1 in the square configuration with tilt −10° and $d/D = 0.96$ (UPM).

however, small differences can be noticed, which are reflected in the performance estimation for this rotor spacing (Fig. 36). The higher velocities estimated by PUMA come from a stronger breaststroke interaction between the front rotors, which results in a greater increase in their efficiency on the advancing side (compared with UPM in Fig. 37). The distribution of the downwash shed from the retreating side of the front rotors in RAMSYS results indicates slightly weaker interaction with back rotors as compared with UPM (Fig. 33(a)). As a result, the estimation of thrust loss for rotors 2 and 4 differed between these tools with RAMSYS predicting roughly 4% smaller thrust reduction for this rotor spacing (Fig. 35).

The differences in predicted wake geometry and propagation do not significantly affect the results at negative tilt angles; however, they lead to greater discrepancies for the backward tilt, where vortices move closer to the rotor planes. This is particularly apparent for the torque values, for which the maximum difference reaches 30% (Fig. 30). As shown in the tandem results, for the tilt angle +10° the wake interactions with the back rotors are the largest, making it the most difficult test case to model. The agreement between high-fidelity code FLOWer and torque measurement improves again for higher angles (Fig. 38), for which the back rotors are no longer located directly in the path of the preceding wake (see the section Discussion). At +10°, the interactions affecting the back rotors are strong regardless of the hub spacing, yet for rotors 1 and 3 they increase significantly for the most compact configurations and so does the discrepancy in the predicted torque values.

Diamond configuration

In the diamond configuration, substantial interactions originate from the diagonal bearhug (rotors 1 and 3) and diagonal breaststroke alignment (rotors 1 and 2). Similar to analyzed two-rotor systems, the performance of rotors 2 and 3 improves due to the influence of tip vortices from rotor 1 from its retreating and advancing side, respectively (Fig. 39). The beneficial effects can already be observed for wider rotor spacings, while it should be noted that in the diamond configuration the distance between side rotors and rotor 1 in the flight direction is shorter than the defined hub distance and is equal to $d/\sqrt{2}$. Additionally, for rotor spacings closer than $1.44D$ the side rotors operate partially behind rotor 1 relative to the flow. As a result, for the closest analyzed hub spacing rotors 2 and 3 operate in conditions comparable to the tandem system and the interactional effects become detrimental to their efficiency.

Rotor 4 is located $\sqrt{2}$ times further from rotor 1 than the distance between front and back rotors in the square configuration. As a result, the influence of the side rotors on rotor 4 is greater than effects of its tandem interaction with rotor 1. The induced velocity fields for −10° tilt presented in Fig. 40 indicate that strong advancing sides interactions between rotors 1, 2, and 4 change the wake propagation of rotor 2 compared with the front rotor. Consequently, in contrast to a beneficial diagonal breaststroke interaction between rotors 2 and 1, rotor 4 is affected by the downwash from rotor 2. This effect, however, is balanced by the influence of the upwash from the retreating side of rotor 3 up to the rotor spacing $1.2D$ (Fig. 41(a)). For closer distances, the influence of both side rotors on rotor 4 becomes disadvantageous (Fig. 41(b)).

In the diamond configuration, differences in the simulated propagation of tip vortices, especially the strong rolled-up vortices from the advancing side, lead to discrepancies in the assessment of interactional effects. As an example, the simulated induced velocity fields for rotor spacing $1.2D$ show that PUMA predicts a stronger and wider vortex shed from the advancing side of rotor 1 in comparison with the UPM outcome (Fig. 40). As a result rotor 2 operates in a strong upwash around azimuth

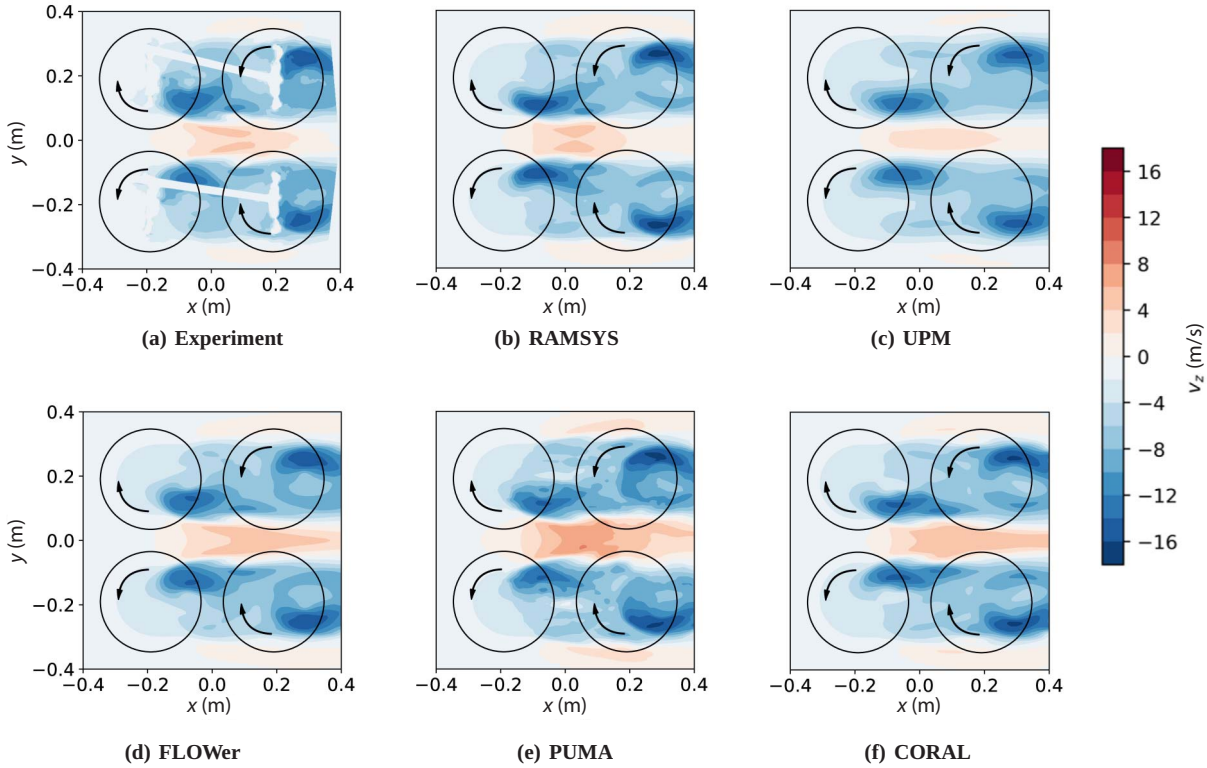

(a) Experiment (b) RAMSYS (c) UPM

(d) FLOWer (e) PUMA (f) CORAL

Fig. 35. Induced velocity fields of the square breaststroke configuration, $d/D = 1.2$, tilt −10°.

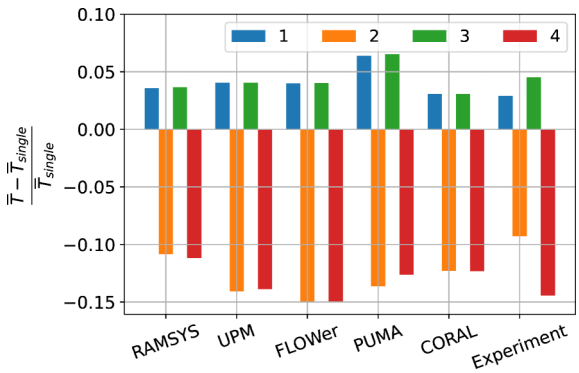

Fig. 36. Change in mean thrust of each rotor in the square breaststroke configuration for $d/D = 1.2$ and tilt angle −10°.

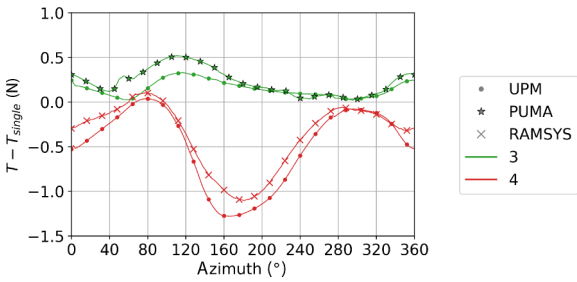

Fig. 37. Relative change in azimuthal blade loading for rotors 3 and 4 in the square breaststroke configuration, $d/D = 1.2$.

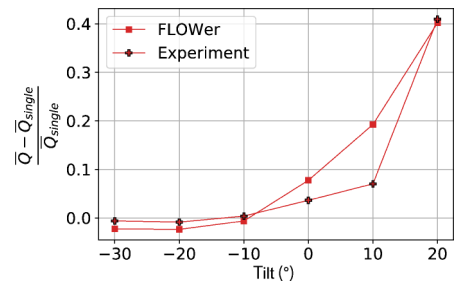

Fig. 38. Relative change of torque of rotor 4 in the square bearhug configuration for $d/D = 1.2$.

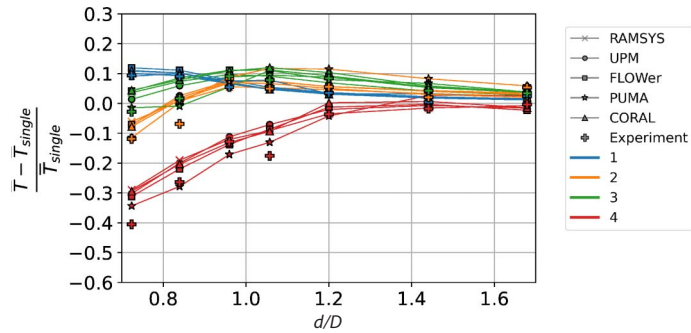

Fig. 39. Change in mean thrust of each rotor in the diamond configuration with varying rotor spacing for tilt angle −10°.

130°, while the same rotor in UPM prediction is affected at 90° azimuth by an inboard downwash of the front rotor, before reaching an upwash region around 150° (Fig. 42). This consequently causes a greater increase of thrust produced by rotor 2 in PUMA calculations with the evaluated relative gain higher by 5% than the UPM result (Fig. 43).

Similarly to square configurations, the increasing tilt angle leads to intensified wake–rotor interactions, especially on rotors 2 and 4, for which

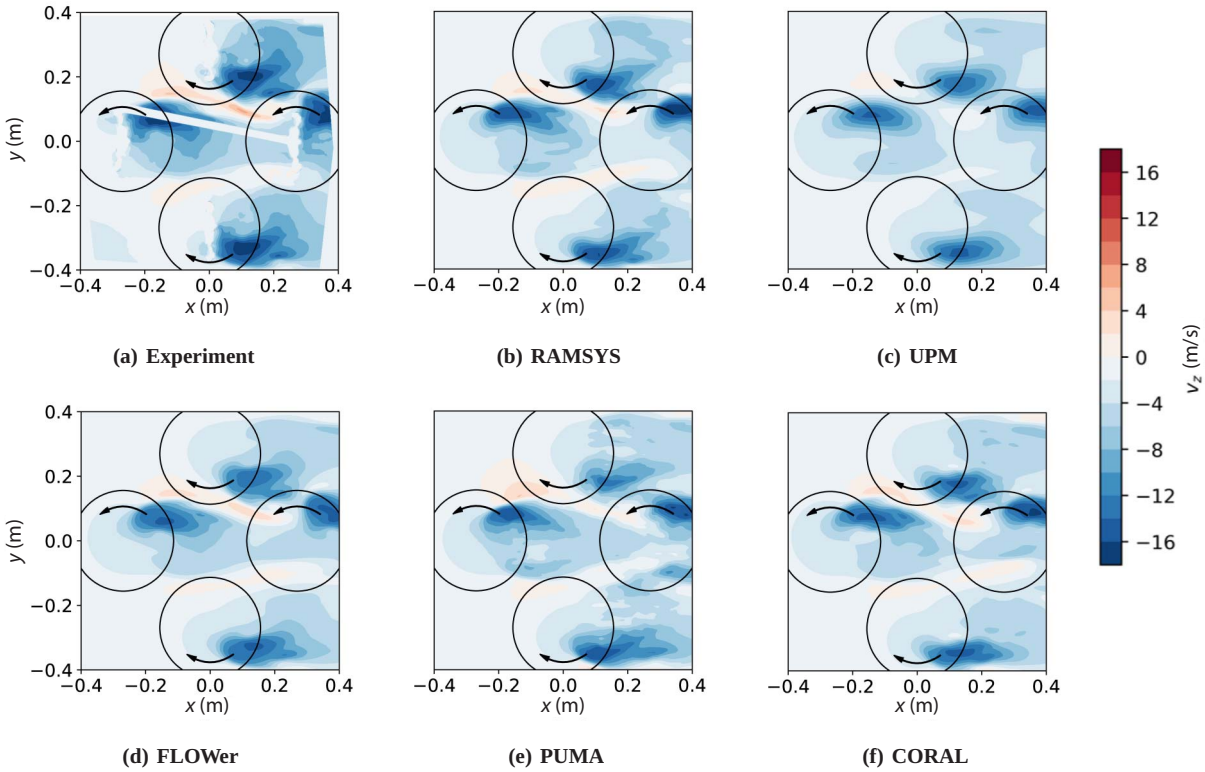

(a) Experiment (b) RAMSYS (c) UPM

(d) FLOWer (e) PUMA (f) CORAL

Fig. 40. Induced velocity fields of the diamond configuration, $d/D = 1.2$, tilt $-10°$.

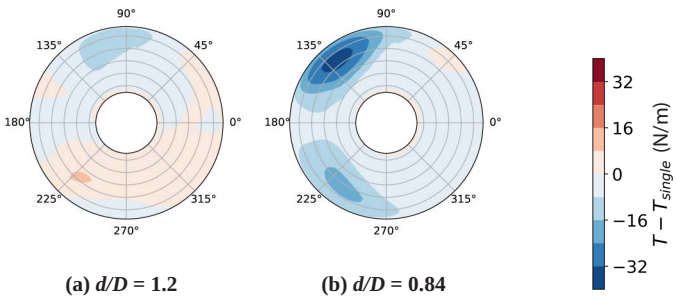

(a) d/D = 1.2 **(b) d/D = 0.84**

Fig. 41. Change in thrust of rotor 4 in the diamond configuration with tilt $-10°$ (UPM).

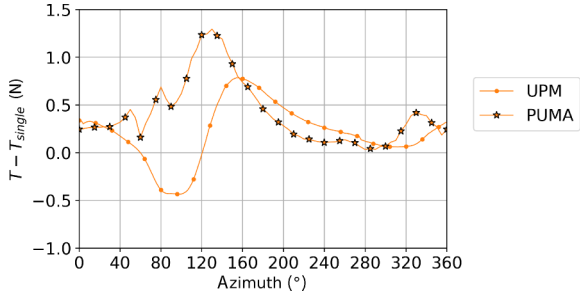

Fig. 42. Relative change in azimuthal blade loading for rotor 2 in the diamond configuration, $d/D = 1.2$.

a wider spread of the calculated values can be observed (Fig. 44). The inviscid methods overestimated the thrust increase on rotor 2 compared to other tools and experimental results, which can indicate that strong

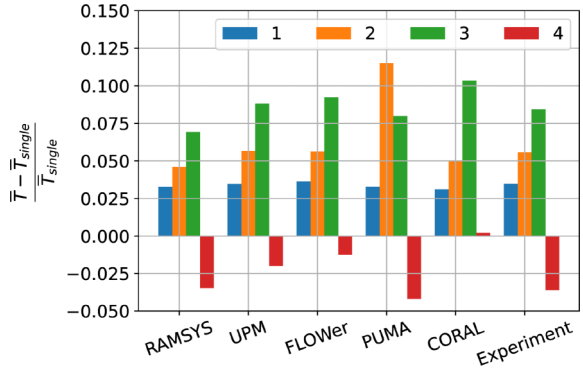

Fig. 43. Change in mean thrust of each rotor in the diamond configuration for $d/D = 1.2$ and tilt angle $-10°$.

upwash from rotor 1 causes a significant increase in angles of attack on rotor 2 leading to local stall regions. Even though the relative change in thrust on the side rotors is similar to cases with a negative tilt, a considerable decrease in their torque can observed for tilt $+10°$ with a minimum at rotor spacing of $1.2D$ (Fig. 45). According to the experimental results, a maximum torque reduction reaches 10% for rotor 3 and almost 30% for rotor 2.

The adverse interactional effects on rotor 4 are worse at tilt $+10°$ causing a drop in its efficiency, however not as much as in the case of back rotors in square configurations. Nevertheless, for overlapping positions, the performance of rotor 4 strongly deteriorates and its thrust loss becomes comparable with that estimated for rotors 2 and 4 in the square system. On the other hand, the efficiency of rotor 1 increases with reduced rotor separations up to 20% due to diagonal bearhug and breaststroke interactions as well as tandem interactions for the closest positioning.

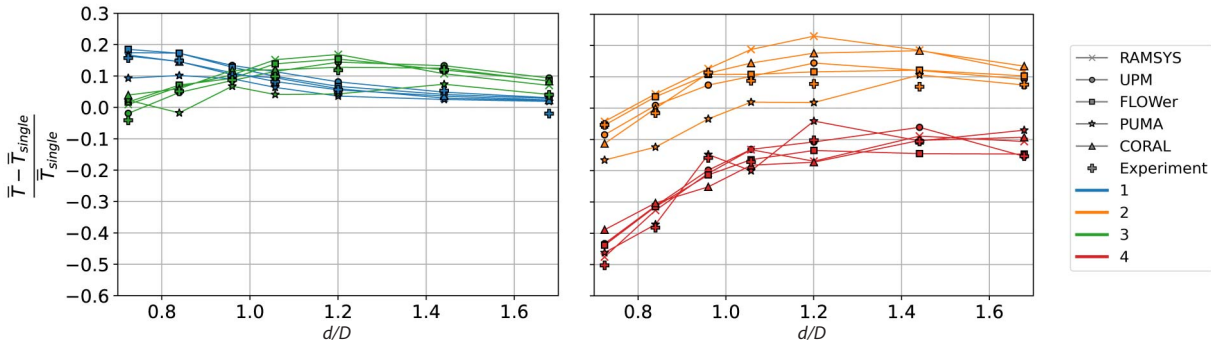

(a) Diamond, rotors 1 and 3 **(b) Diamond, rotors 2 and 4**

Fig. 44. Change in mean thrust of each rotor with varying rotor spacing for tilt angle +10°.

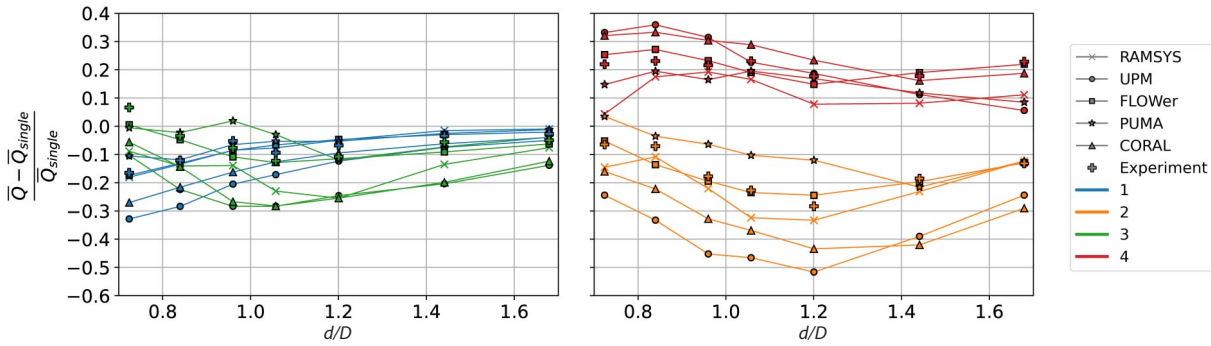

(a) Diamond, rotors 1 and 3 **(b) Diamond, rotors 2 and 4**

Fig. 45. Change in mean torque of each rotor with varying rotor spacing for tilt angle +10°.

Discussion

Rotor efficiency

The interactional effects were evaluated based on the changes in the thrust and torque values, which are, with the latter implicating a change in the power consumption, the most important parameters in the assessment of the UAV's performance. The rotor efficiency in the forward flight was evaluated from the power loading defined as

$$\frac{T}{P} = \frac{T}{Q\omega}. \tag{1}$$

An improvement in the rotor efficiency due to interactions was observed for the cases with increased thrust and simultaneously reduced torque, characteristic of side rotors in the diamond configuration. In practice, the resulting excess of the thrust would be compensated with a decrease in the rotor rotational speed. Nevertheless, the qualitative conclusion remains the same, as this in turn implicates further reduction of the required power at a given rotor thrust. A similar observation applies to the cases with a drop in the efficiency (e.g., back rotors in the square configurations).

Accuracy of the measurement

The accuracy of the thrust measurement can be estimated from the balance calibration from different days. Assuming that the variation of the thrust measurement should only occur proportionally due to changes in the air density, the calculated uncertainty equals 3.8% for rotor 1, 1.4% for rotor 2, 1.5% for rotor 3, and 1.9% for rotor 4. Possible errors due to the balance drift in the measured absolute thrust differences were minimized by repeating single rotor measurements directly before multirotor test cases. The standard deviation of the thrust from the isolated rotor measurements on different days equals 0.2 N for -10° tilt and 0.3 N for $+10^\circ$, which is around 3% of the average value for both cases. The deviation for the torque values equals 0.001 Nm, which lies below 2% for both tilt angles. The torque coefficient of a single rotor derived from the electric power matches with the measurements done using a piezoelectric balance from the previous campaign, within the experimental error (Refs. 28, 37).

Another uncertainty of the results can be evaluated based on the symmetry accuracy. By concept, the square configuration is symmetric, which means that both front and back rotors should produce the same forces. Deviations from this rule seen in the results can occur due to the uncertainty of the measuring devices, geometry imperfections, and asymmetry in the flow. Based on the average of the measurements from different days, the difference in thrust measurement of the front rotors (1 and 3) equals 0.25 N regardless of the tilt angle, while for the back rotors (2 and 4) the difference equals 0.16 N for -10° tilt and it raises to 0.3 N for $+10^\circ$ tilt. The measured torque differed by 0.001 Nm between the front rotors and 0.006 Nm between the back rotors.

Discrepancies in torque prediction

Figure 46 presents the change in torque of rotor 2 from Figs. 19(b) and 22(b) as the absolute difference from an isolated rotor results. Potential methods, like UPM, are capable of capturing the trends in torque changes

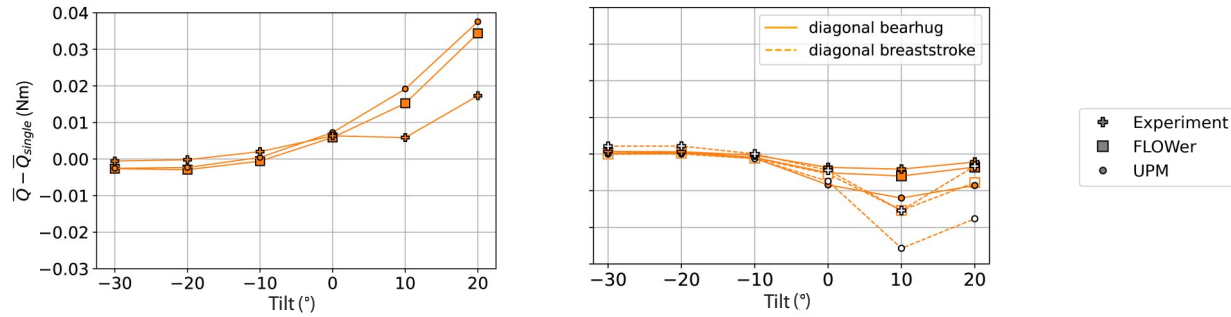

(a) Tandem **(b) Oblique alignment**

Fig. 46. Absolute torque change of rotor 2 for $d/D = 1.2$.

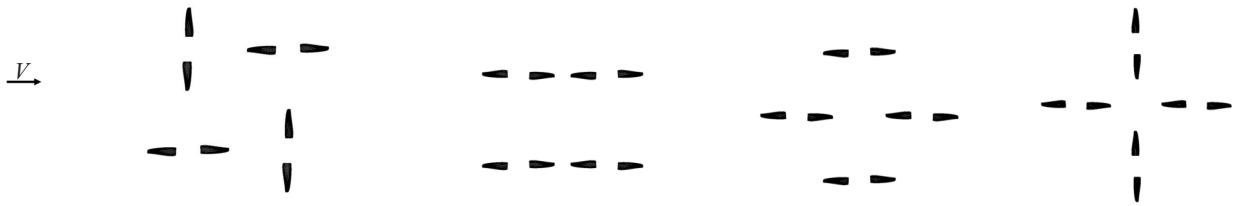

(a) Square, orthogonal phasing **(b) Square, tip-to-tip phasing** **(c) Diamond, orthogonal phasing** **(d) Diamond, tip-to-tip phasing**

Fig. 47. Analyzed rotor phasing in quadrotor configurations.

due to interactions comparable with high-fidelity results (Fig. 46(a)). Nevertheless, as these tools do not account for the viscous drag and thus underestimate the absolute torque values, the resulting relative torque changes can be strongly overestimated. This is apparent especially for tandem interactions (and, therefore, also for square configurations) at high backward tilt angles, for which the torque on the back rotors strongly increases with the reference torque of a single rotor declining. Additionally, as shown in Fig. 46(a), while UPM and FLOWer results show comparable tendency for the whole range of tilt angles, the measurement indicates a change in the observable trend at 10°. As the interactions with the rear rotor are the strongest at this angle for the tandem configuration, it is expected that any inconsistency with the experimental setup, like the exact tilt angle, would cause notable discrepancies between the measurement and computational results for this case, especially when it comes to torque, sensitive to the exact onflow conditions. As a result, also for square configurations most of the tools, including high-fidelity solver FLOWer, overestimate torque increase on the back rotors at 10° compared to the measurement (Fig. 30).

The agreement of the predicted torque trends between potential tool UPM and FLOWer is worse at backward rotor tilt for oblique alignment interactions (Fig. 46(b)), which indicates the influence of viscous effects. In these cases, unlike in the tandem configuration, angles of attack on rotor 2 are locally increased by the upwash from the wake of the front rotor. At higher tilt angles, this leads to flow separation and thus viscous drag increase, which cannot be predicted by potential methods. The resulting discrepancy between UPM results and FLOWer/ experiment is more significant for a diagonal breaststroke interaction, as it affects the advancing side of rotor 2 producing most of the rotor forces. Analogically, potential methods (UPM, RAMSYS, CORAL) tend to overestimate torque reduction for side rotors 2 and 3 in the diamond configuration, as shown for 10° tilt angle (Fig. 45). A similar observation applies to side-by-side interactions at high tilt angles.

Calculations performed with potential solver PUMA considered the viscous effects through airfoil characteristics. This approach did not always bring the improvement in the performance prediction due to uncertainty in the airfoil data for low Reynolds numbers or reduced accuracy of the polars for higher angles of attack. Therefore, taking an example of the diamond configuration, PUMA results indicate stronger upwash on rotor 2 leading to a greater stall on its blades (Fig. 45).

Discrepancies between UPM and RAMSYS results for the square configurations at 10° tilt angle prove that for high-interaction cases, differences in the wake propagation between the solvers can have a greater impact than viscous versus potential flow assumptions or different blade representations (Fig. 30).

Relevance of rotor phasing

The presented results were prepared with an assumption of orthogonal rotor phasing, which was necessary for the test cases with overlapping blades. For selected nonoverlapping rotor spacing $d/D = 1.2$, measurements were performed for both orthogonal and tip-to-tip rotor phasing (Fig. 47). The comparison of the results obtained for the diamond configuration indicates that rotor phasing has a negligible influence on thrust and torque produced by the quadrotor for the whole range of analyzed tilt angles (Fig. 48). Nevertheless, as shown in (Refs. 22, 23), the rotor phasing can be a decisive factor in the aeroacoustic design.

Conclusions

The nature of interactional effects on quadrotor performance in forward flight was explained based on the investigation of two-rotor systems. The analysis indicates the tandem alignment has a strong, detrimental influence on the rear rotors operating in the downwash from the preceding rotors. The tandem interactions intensify with increasing tilt angle, leading to a thrust reduction of up to 40% with the simultaneous increase in produced torque. The back rotors may be positively affected if positioned in the oblique alignment where they operate in the upwash

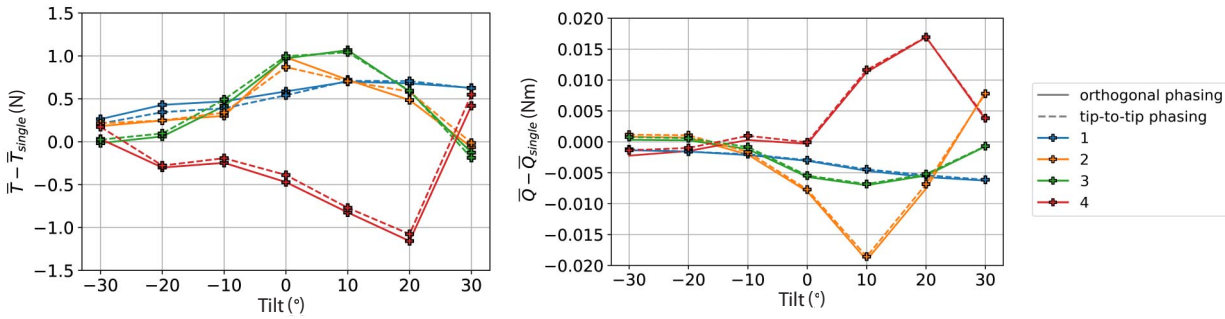

(a) Thrust **(b) Torque**

Fig. 48. Absolute changes of rotor thrust and torque in the diamond configuration depending on the rotor phasing, $d/D = 1.2$.

regions caused by the rolled-up tip vortices of the preceding rotors. The beneficial effects could also be observed for side-by-side interactions for closer spacings, with the breaststroke system being more favorable.

The tandem interaction is dominant in square configurations, where for all analyzed rotor spacings the square systems produce less thrust than isolated rotors. For higher tilt angles, the deteriorating effects worsen and the efficiency continues to decrease. Rotor separations with slightly overlapping blades are the most advantageous as the efficiency of front rotors increases, and the back rotors are positively affected by the side-by-side interactions. The performance of the diamond system is determined by the diagonal bearhug and breaststroke interactions improving the system performance by up to 5% compared with isolated rotors for all nonoverlapping rotor spacings. For the tilt angle $+10°$, further benefits can be observed due to a decrease in produced torque on the side rotors resulting in the 10% efficiency increase.

The computational results showed good agreement with the measurement data for the forward rotor plane tilt; however, for the increased rotor–wake interactions at a backward tilt angle, the spread between the calculated values, especially for torque, could be observed with the general trends maintained.

It should be noted that for the fixed-pitch quadrotors, controlled by the variable RPM, the overlapping positions require a vertical separation between the front and back rotors. The possible change in the interactional effects of such alignment is a topic for future investigation.

Acknowledgments

The study was funded by the German Aerospace Center (DLR) as a part of the Urban Rescue project. Cooperation between research facilities was enabled within the group GARTEUR AG-25 "Rotor-rotor Wakes Interactions." The first author would like to greatly acknowledge the support of Dr. Christian Wolf in setting up the PIV measurement.

References

[1]Shukla, D., and Komerath, N., "Multirotor Drone Aerodynamic Interaction Investigation," *Drones*, **2**, 43 (2018), DOI:10.3390/drones2040043.

[2]Shukla, D., and Komerath, N., "Low Reynolds Number Multirotor Aerodynamic Wake Interactions," *Experiments in Fluids*, **60**, 77 (2019), DOI: 10.1007/s00348-019-2724-3.

[3]Hwang, J. Y., Jun, M. K., and Kwon, O. J., "Numerical Study of Aerodynamic Performance of a Multirotor Unmanned-Aerial-Vehicle Configuration," *Journal of Aircraft*, Vol. 52, (3), May–June 2015, pp. 839–846, DOI: 10.2514/1.C032828.

[4]Barcelos, D., Kolaei, A., and Bramesfeld, G., "Aerodynamic Interactions of Quadrotor Configurations," *Journal of Aircraft*, Vol. 57, (6), November–December 2020, pp. 1074–1090, DOI: 10.2514/1.C035614.

[5]Healy, R., Misiorowski, M., and Gandhi, F., "A CFD-Based Examination of Rotor-Rotor Separation Effects on Interactional Aerodynamics for eVTOL Aircraft," *Journal of the American Helicopter Society*, **67**, 012006 (2022), DOI: 10.4050/JAHS.67.012006.

[6]Throneberry, G., Takeshita, A., Hocut C., Shu, F., and Abdelkefi, A., "Wake Propagation and Characteristics of a Multi-Rotor Unmanned Vehicle in Forward Flight," *Drones*, **6**, 130 (2022), DOI: 10.3390/drones6050130.

[7]Misiorowski, M., Gandhi, F., and Oberai, A. A., "A Computational Study on Rotor Interactional Effects in Edgewise Flight," *AIAA Journal*, Vol. 57, (12), December 2019, pp. 5309–5319, DOI: 10.2514/1.J058369.

[8]Niemiec, R., and Gandhi, F., "A Comparison between Quadrotor Flight Configurations," Proceedings of the 42nd European Rotorcraft Forum, Lille, France, September 5–8, 2016.

[9]Atte A., Wylie, D., and Rauleder, J., "Experimental Evaluation of Multi-Rotor Aerodynamic Interactions," Proceedings of the 78th Annual Forum of the American Helicopter Society, Fort Worth, TX, May 10–12, 2022, DOI: 10.4050/F-0078-2022-17467.

[10]Ventura, Diaz P., and Yoon, S., "High-Fidelity Computational Aerodynamics of Multi-Rotor Unmanned Aerial Vehicles," Proceedings of the AIAA SciTech Forum 2018, Kissimmee, FL, January 8–12, 2018, DOI: 10.2514/6.2018-1266.

[11]Healy, R., Gandhi, F., and Mistry, M., "Computational Investigation of Multirotor Interactional Aerodynamics with Hub Lateral and Longitudinal Canting," *AIAA Journal*, Vol. 60, (2), February 2022, pp. 872–882, DOI: 10.2514/1.J060530.

[12]Lee, J., Lee, K., and Oh, S., "Aerodynamic Characteristic Analysis of Multi-Rotors Using a Modified Free-Wake Method," *Transactions of the Japan Society for Aeronautical and Space Sciences*, Vol. 52, (177), 2009, pp. 168-179, DOI: 10.2322/tjsass.52.168.

[13]Piccinini, R., Tugnoli, M., and Zanotti, A., "Numerical Investigation of the Rotor-Rotor Aerodynamic Interaction for eVTOL Aircraft Configurations," *Energies*, **13**, 5995 (2020), DOI: 10.3390/en13225995.

[14]Chen, G. H., Nunez, G. F., Russel, C. R., Avera, M. P., and Dotterweich, J. M., "Wind Tunnel Test Results for an Overlapped Quadrotor Configured UAS," Proceedings of the 74th Annual Forum of the American Helicopter Society, Phoenix, AZ, May 14–17, 2018.

[15]Jia, Z., and Lee, S., "Computational Study on Noise of Urban Air Mobility Quadrotor Aircraft," *Journal of the American Helicopter Society*, **67**, 012009 (2022), DOI: 10.4050/JAHS.67.012009.

[16]Jia Z., and Lee S., "Aeroacoustic Analysis of Side-by-side Hybrid VTOL Aircraft," Proceedings of the 76th Annual Forum of the American Helicopter Society, Virtual, October 5–8, 2020, DOI: 10.4050/F-0076-2020-16491.

[17]Zhou, W., Ning, Z., Li, H., and Hu, H., "An Experimental Investigation on Rotor-to-Rotor Interactions of Small UAV," Proceedings of the 35th AIAA Applied Aerodynamics Conference, Denver, CO, June 5–9, 2017, DOI: 10.2514/6.2017-3744.

[18]Lee, H., and Lee, D.-J., "Rotor Interactional Effects on Aerodynamic and Noise Characteristics of a Small Multirotor Unmanned Aerial Vehicle," *Physics of Fluids*, **32**, 047107 (2020), DOI: 10.1063/5.0003992.

[19]Ko, J., Kim, J., and Lee, S., "Computational Study of Wake Interaction and Aeroacoustic Characteristics in Multirotor Configurations," Proceedings of the INTER-NOISE and NOISE-CON Congress and Conference, Madrid, Spain, June 16–19, 2019.

[20]Intaratep, N., Alexander, W., Devenport, W., Grace, S., and Dropkin, A., "Experimental Study of Quadcopter Acoustics and Performance at Static Thrust Conditions," Proceedings of the 22nd AIAA/CEAS Aeroacoustic Conference, Lyon, France, May 30–June 1, 2016, DOI: 10.2514/6.2016-2873.

[21]Tinney, C., and Sirohi, J., "Multirotor Drone Noise at Static Thrust," *AIAA Journal*, Vol. 56, (7), July 2018, pp. 2816–2826, DOI:10.2514/I.J056827.

[22]Zhou, T., and Fattah, R., "Tonal Noise Characteristics of Two Small-Scale Propellers," Proceedings of the 23rd AIAA/CEAS Aeroacoustics Conference, Denver, CO, June 5–9, 2017, DOI: 10.2514/6.2017-4054.

[23]Smith, B., Gandhi, F., and Niemiec, R., "A Comparison of Multicopter Noise Characteristics with Increasing Number of Rotors," Proceedings of the 76th Annual Forum of the American Helicopter Society, Virtual, October 5–8, 2020.

[24]Yoon, S., Diaz, P., Boyd, D., Jr., Chan, W., and Theodore, C., "Computational Aerodynamic Modeling of Small Quadcopter Vehicles," Proceedings of the 73rd Annual Forum of the American Helicopter Society, Fort Worth, TX, May 9–11, 2017.

[25]Niemiec, R., and Gandhi, F., "Effects of Inflow Model on Simulated Aeromechanics of a Quadrotor Helicopter," Proceedings of the 72 Annual Forum of the American Helicopter Society, West Palm Beach, Florida, May 17–19, 2016.

[26]Pinti, O., Oberai, A. A., Healy, R., Niemiec, R. J., and Gandhi, F., "Multi-Fidelity Approach to Predicting Multi-Rotor Aerodynamic Interactions," *AIAA Journal*, Vol. 60, (6), June 2022, pp. 3894–3908, DOI: 10.2514/I.J060227.

[27]Conley, S., and Shirazi, D. "Comparing Simulation Results from CHARM and RotCFD to the Multirotor Test Bed Experimental Data," Proceedings of the AIAA Aviation Forum, Virtual, August 2–6, 2021, DOI: 10.2514/6.2021-2540.

[28]Kostek, A. A., Lößle F, Wickersheim, R., Keßler M., Boisard, R., Reboul, G., Visingardi, A., Barbarino, M., and Gardner, A. D., "Experimental Investigation of UAV Aerodynamics and Aeroacoustics with Computational Cross-Validation," *CEAS Journal*, Vol. 14, (3), 2023, pp. 1–16, DOI: 10.1007/s13272-023-00680-z.

[29]Boisard, R., Lefevre, L., Zhang, T., Barakos, G., Visingardi, A., Lößle, F., Kostek, A., Andronikos, T., Keßler, M., Wickersheim, R., Colli, A., Gibertini, G., and Zanotti, A., "Rotor/Rotor Aerodynamic Interactions - A Garteur Group," Proceedings of the 33rd Congress of the International Council of the Aeronautical Sciences, Stockholm, Sweden, September 4–9, 2022.

[30]Ahmed, S.R., and Vidjaja, V.T., "Unsteady Panel Method Calculation of Pressure Distribution on BO 105 Model Rotor Blades," *Journal of the American Helicopter Society*, Vol. 43, (1), 1998, pp. 47–56, DOI: 10.4050/JAHS.43.47.

[31]Visingardi, A., D'Alascio, A., Pagano, A., and Renzoni, P., "Validation of CIRA's Rotorcraft Aerodynamic Modelling System with DNW Experimental Data," Proceedings of the 22nd European Rotorcraft Forum, Brighton, UK, September 16–19, 1996.

[32]Morino, L., "A General Theory of Unsteady Compressible Potential Aerodynamics," NASA CR-2464, 1974, DOI: 10.1007/978-3-662-06153-4_27.

[33]Mudry, M., "La théorie des nappes tourbillonnaires et ses applications à l'aérodynamique instationnaire," Ph.D. thesis, University of Paris VI, 1982.

[34]Nitzsche, F., Spieß C., Leibbrandt, R., Gennaretti, M., Bernardini, G., Serafini, J., Porcacchia, F., Riziotis, V., Papadakis, G., Spyropoulos, N., Siami, A., Hilewit, D., and Rafiee, M., "A New Comprehensive Analysis Tool for the Preliminary Design and Design Evaluation of Helicopters: – The CORAL," Proceedings of the 47th European Rotorcraft Forum, Virtual, September 7–9, 2021.

[35]Kroll, N., Rossow, C. C., Becker, K., and Thiele, F., "MEGAFLOW—A Numerical Flow Simulation System," Proceedings of the 21st ICAS Congress, Melbourne, Australia, September 13–18, 1998, pp. 13-09.

[36]Wilcox, D. C., "Multiscale Model for Turbulent Flows," *AIAA Journal*, Vol. 26, (11), November 1988, pp. 1311–1320, DOI: 10.2514/3.10042.

[37]Lößle F., Kostek, A.A., Schwarz, C., Schmid, R., Gardner, A.D., and Raffel, M., "Aerodynamics of Small Rotors in Hover and Forward Flight," Proceedings of the 48th European Rotorcraft Forum, Winterthur, Switzerland, September 6-8, 2022.